Immunogenic cell death-related cancer-associated fibroblast clusters and prognostic risk model in cervical cancer

Fei Wu and Yue Xu[a] (iD)

AFFILIATIONS

Department of Obstetrics and Gynecology, The Second Hospital of Jilin University, Changchun 130000, Jilin, China

[a]Author to whom correspondence should be addressed: xuyue2010@jlu.edu.cn

ABSTRACT

Cervical cancer (CC) remains a leading cause of female cancer mortality globally. Immunogenic cell death (ICD) influences the tumor microenvironment (TME) and adaptive immune responses. Cancer-associated fibroblasts (CAFs) within the TME suppress anti-tumor immunity and contribute to CC progression. This study identified three ICD-related CAF clusters linked to patient survival, including IL6+CAF and ILR1+CAF, which were associated with clinical outcomes. Using a nine-gene risk model, patients were stratified into risk groups, with high-risk individuals showing worse survival and correlations with pathways such as hypoxia and TGFβ. The model also predicted immunotherapy responses, highlighting immune infiltration differences across risk groups. These findings provide insights into the role of CAF clusters in CC and present a risk model that supports prognosis prediction and personalized therapy.

INTRODUCTION

Cervical cancer (CC) is the fourth most common cancer among women globally, with more than 600 000 new cases in 2020 and over 340 000 deaths, accounting for nearly 8% of all female cancer deaths yearly.[1–3] HPV, a human papillomavirus, is necessary to develop CC.[4] However, up to 5% of CCs are not associated with HPV-persistent infection.[5] The introduction of HPV vaccines has made substantial advancements to CC treatment.[6–8] Nevertheless, CC remains a critical healthcare concern, especially in low- to middle-income countries.[9] Furthermore, the molecular pathways driving CC are still unknown. It is thus critical to develop reliable risk models for CC that can help with prognostic prediction and personalized treatment.

Immunogenic cell death (ICD) can modify tumor immunological microenvironments by generating warning signals, making immunotherapy more effective.[10,11] In combination with non-ICD-inducing chemotherapeutic agents like cisplatin and crizotinib, an ICD-inducing tyrosine kinase inhibitor has exceptional anti-tumor activity.[12] Preclinical evidence indicates that cytotoxic agents that induce ICD (such as oxaliplatin and cyclophosphamide) can improve immunotherapy.[13] In CC, Wu et al. induced ICD by triggering endoplasmic reticulum stress in human CC cells for anti-tumor treatment.[14] ICD boosts anticancer immune responses by converting dying cancer cells into therapeutic immunotherapies. Tumors with a higher ICD propensity may elicit a stronger anti-tumor immune response, aiding in anti-tumor progression.

Tumor cells and stromal cells constitute the tumor microenvironment, and their dynamic interaction contributes to the development of cancer.[15,16] Cancer-associated fibroblasts (CAFs) support tumorigenesis by stimulating angiogenesis.[17] CAFs comprise a significant proportion of the stromal cells and promote tumor growth. CAFs were associated with immune regulation and metastasis in CC.[18,19] Qu et al. identified pro-tumorigenic cancer-associated myofibroblasts (myCAFs) cluster by sing-cell RNA sequencing (scRNA-seq) technology in advanced CC.[20] Li et al. distinguished inflammatory CAFs (iCAFs) in CC that promote tumor progression.[21] Sheng et al. discovered that CAF clusters induced radioresistance in CC by promoting macrophage toward the M2 phenotype polarization.[22] Of note, the characteristic of CAFs in generating extracellular matrix components and producing secreted exosomes, metabolites, cytokines, and chemokines that influence tumor metabolism, immunology, and angiogenesis, which made the CAFs a key pro-tumorigenic effects.[16,23,24] Thus, a thorough analysis of the tumor-promoting and tumor-restraining roles of CAF subtypes, particularly how these intricate capabilities originate and are regulated by neoplastic cells throughout cancer progression,

may aid in the creation of innovative diagnostic and therapeutic strategies.

Here, we identified a risk model for CC based on ICD-related CAF clusters. A unique nomogram was developed to assist the practical use of CAFs in prognosis prediction. It might lead to more customized therapies and better results for CC patients by providing fresh insights into tumor pathogenesis. A better understanding of CAF biology will shed light on a novel therapeutic strategy against CC.

RESULTS

ICD score analysis and ICD-related CAF clusters identification

We obtained 19 510 cells from four CC patients. After harmony to remove batch effects, as demonstrated in the supplementary material, Figs. 1(a) and 1(b), the seven samples were successfully integrated. 26 clusters were found after dimensionality reduction [supplementary material, Fig. 1(c)]. We categorized the cells into eleven major clusters using marker genes for distinct cell types, including endothelial cells, smooth muscle cells, fibroblasts, T cells, monocytes/macrophages, plasma cells, epithelial cells, neutrophils, mast cells, and NK cells [Fig. 1(a)]. The heatmap shows the top five gene markers for each cell type [Fig. 1(b)]. We used the "AddModuleScore" function to calculate the ICD score in different cell types. The ICD scores of the eleven cell types were demonstrated [Fig. 1(c)]. Immune cell types such as T cells, monocytes/macrophages, and mast cells had considerably higher ICD scores [Fig. 1(d)]. In addition, we found significantly elevated ICD scores in the tumor [supplementary material, Fig. 1(d)]. The ICD scores of fibroblasts in tumors were much higher than those in normal samples [Fig. 1(e)]. Since the CAFs can affect tumor progression, the fibroblasts in the tumor group were extracted for re-clustering with the non-negative matrix factorization (NMF) method based on the ICD-related genes. Finally, 5 CAF subclusters were identified [Fig. 1(f)]. Then, we analyzed marker genes of each subcluster [supplementary material, Fig. 1(e)], based on which the CAF clusters were identified, including Non-ICD-CAF-C1, IFNGR1+CAF-C2, Non-ICD-CAF-C3, ILR1+CAF-C4, and IL6+CAF-C5 [Fig. 1(g)]. The proportion of the 5 CAF clusters in each tumor sample is demonstrated in Fig. 1(h). The feature plots of the three ICD genes (IFNGR1, ILR1, and IL6) are illustrated in the supplementary material, Fig. 1(f).

Pseudotime trajectory analysis of the ICD-related CAF clusters

The pseudotime trajectory analysis was used to further understand how distinct ICD-related CAF clusters developed in CC. First, CytoTRACE analysis was used to predict the ordering of the 5 CAF clusters. Fig. 2(a) demonstrates the distribution of predicted order in the CAF clusters, with IL6+CAF and ILR1+CAF showing more red-point concentration as frontward orders. The CytoTRACE scores are higher in IL6+CAF and ILR1+CAF than in other CAF clusters, indicating a low level of differentiation and suggesting that these cells are the starting point within these CAF clusters [Fig. 2(b)]. Then, with monocle analysis for a detailed examination, our results showed that the CAF clusters were classified into seven states. Pseudotime also showed that IL6+CAF and ILR1+CAF were at the relative beginning of the trajectory path with a lighter shade of red in the pseudotime progress, whereas the Non-ICD-CAF clusters of C1 and C3 were at a

relative terminal state [Fig. 2(c)]. In addition, the Non-ICD-CAF clusters enriched more in states 1, 2, and 7, while the IL6+CAF and ILR1+CAF enriched in states 3–6 [Figs. 2(d)–3(f)]. Of interest, the ridge map demonstrated the IL6+CAF was highly enriched in the middle of the pseudotime [Fig. 2(g)], indicating an important role in tumor biological regulation. The heat map showed the related biological processes in the pseudotiome and states among the five CAFs, including extracellular matrix organization, response to lipopolysaccharide, and DNA-binding transcription [Fig. 2(h)]. Finally, we conducted a Branched Expression Analysis Modeling (BEAM) analysis of the 32 ICD-related genes in the pseudotime. ENTPD1, TLR4, and MYD88 were elevated at the beginning of the pseudo-temporal trajectory [Fig. 2(i)], which are pivotal in immune responses, inflammation, and infection control. Furthermore, at the end of the pseudo-temporal trajectory, NT5E and P2RX7 were found elevated. NT5E encodes for the enzyme CD73, which is crucial in purine metabolism.[25] P2RX7 also encodes the purinergic receptor family and contributes to an essential aspect of cellular communication.[26] The observation indicates that the CAF clusters undergo distinct differentiation processes, suggesting different physiological functions in CC.

Identification of prognostic value and functional characteristics of CAFs

We first determined the marker genes of the five CAFs (supplementary material, Table III). Then, ssGSEA score enrichment of the marker genes of each CAF cluster was applied to the bulk datasets. The findings revealed that the IFNGR1+CAF cluster, IL6+CAF cluster, and Non-ICD-CAF-C3 cluster were linked to CC patients' survival [Fig. 3(a)]. Patients in the low-CAF score group survived better than those in the high-CAF score group for the three clusters. As a stromal component that affects the TME, CAFs secrete various growth factors and cytokines and degrade extracellular matrix proteins, thereby affecting tumor cell proliferation, metastasis, and chemotherapy resistance. Then, we analyzed the functional characteristics of the 5 CAF clusters. The correlation of the 5 CAFs is illustrated in Fig. 3(b). Based on a prior study's estimation of Pan-CAF signatures,[27] we discovered that IL6+CAF was substantially linked to inflammatory CAF (iCAF) [Fig. 3(c)], which were reported to be located far from tumor cells in the desmoplastic area.[28] The IL1R1+CAF resembled developmental CAF (dCAF, related to stem cell character)[29] and pCAF (Pdpn marked, related to wound healing and immune regulation).[30] Non-ICD-CAF clusters had the myofibroblastic CAF (myCAF) characteristics, which were found to be located near tumor cell nests.[31,32] We utilized GSVA to examine the association between CAF clusters and distinct pathways and discovered that 30 metabolic pathways varied substantially across the five CAF clusters [Fig. 3(d)]. The IFNGR1+CAF had more metabolic pathways related to energy production, immune responses, and lipid metabolism. The IL6+CAF had more metabolic pathways related to pyruvate metabolism, which enables energy production under anaerobic conditions.[33] The 10 hallmark pathways then showed markedly varied activity across the five clusters [Fig. 3(e)], and we found that the IL6+CAF highly related to HALLMARK_TNFA_SIGNALING_VIA_NFKB, which is involved in various cellular processes, including immune and inflammatory responses.[34] Furthermore, different activations of putative TFs were shown among
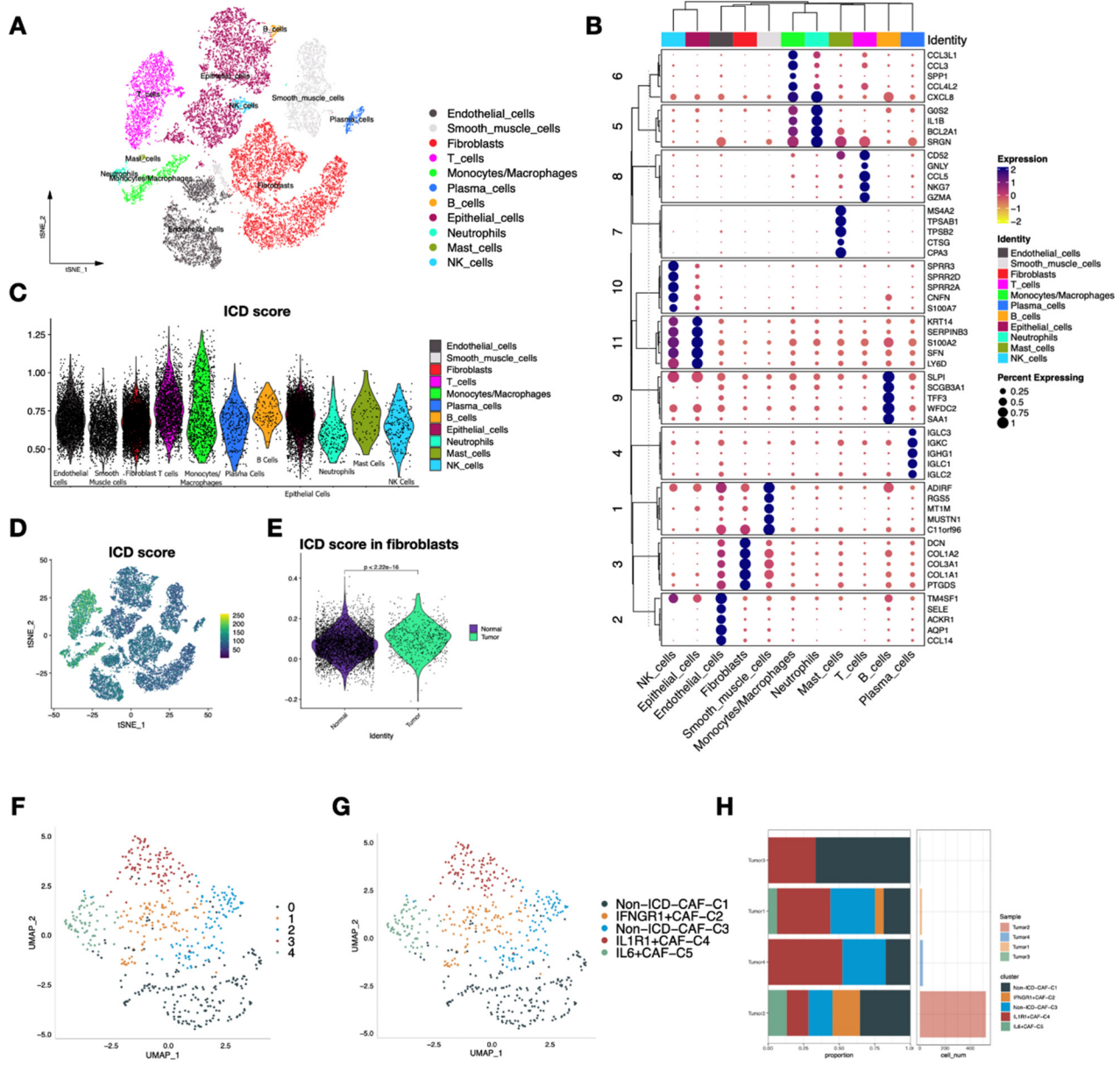
FIG. 1. ICD score analysis and ICD-related CAF cluster identification. (a) The tSNE plot of 11 cell types. (b) Dot plot showing top 5 marker genes for 11 cell types. (c) ICD score in the 11 cell types. The distribution (d) and comparison (e) of ICD scores. (f, g) The UMAP plot of 5 CAF clusters. (h) The proportion of the 5 CAF clusters in the tumor samples.

CAF clusters according to the SCENIC analysis [Fig. 3(f)], from which the NFKB family regulators were highly enriched in IL6+CAF.

Cell chat analysis of prognostic CAFs

Since the dynamic crosstalk between cancer cells and CAFs promotes cancer progression, we performed cell chat analysis of the two prognostic ICD-related CAF clusters. We found that the two clusters (IFNGR1+CAF cluster, IL6+CAF cluster) had the most interactions with epithelial cells in tumor samples [Figs. 4(a)–5(c)], indicating their

crucial role in TME regulation and tumor progression. The outgoing interaction strength of IFNGR1+CAF and IL6+CAF ranked among the highest compared to all other cells. Then, we analyzed potential pathways involved in the two CAF clusters and found COLLAGEN, PTN, and MK signaling were highly enriched in the outgoing communication of the two CAFs [Fig. 4(d)]. The Sankey diagram demonstrated that IFNGR1+CAF and IL6+CAF had similar secreting patterns [Fig. 4(e)]. Among these pathways, MK participates in the epithelial-to-mesenchymal (EMT) activities that are essential for signal transduction as a bridge in the translation from extracellular stimuli to a variety of cellular signals.[35] From our
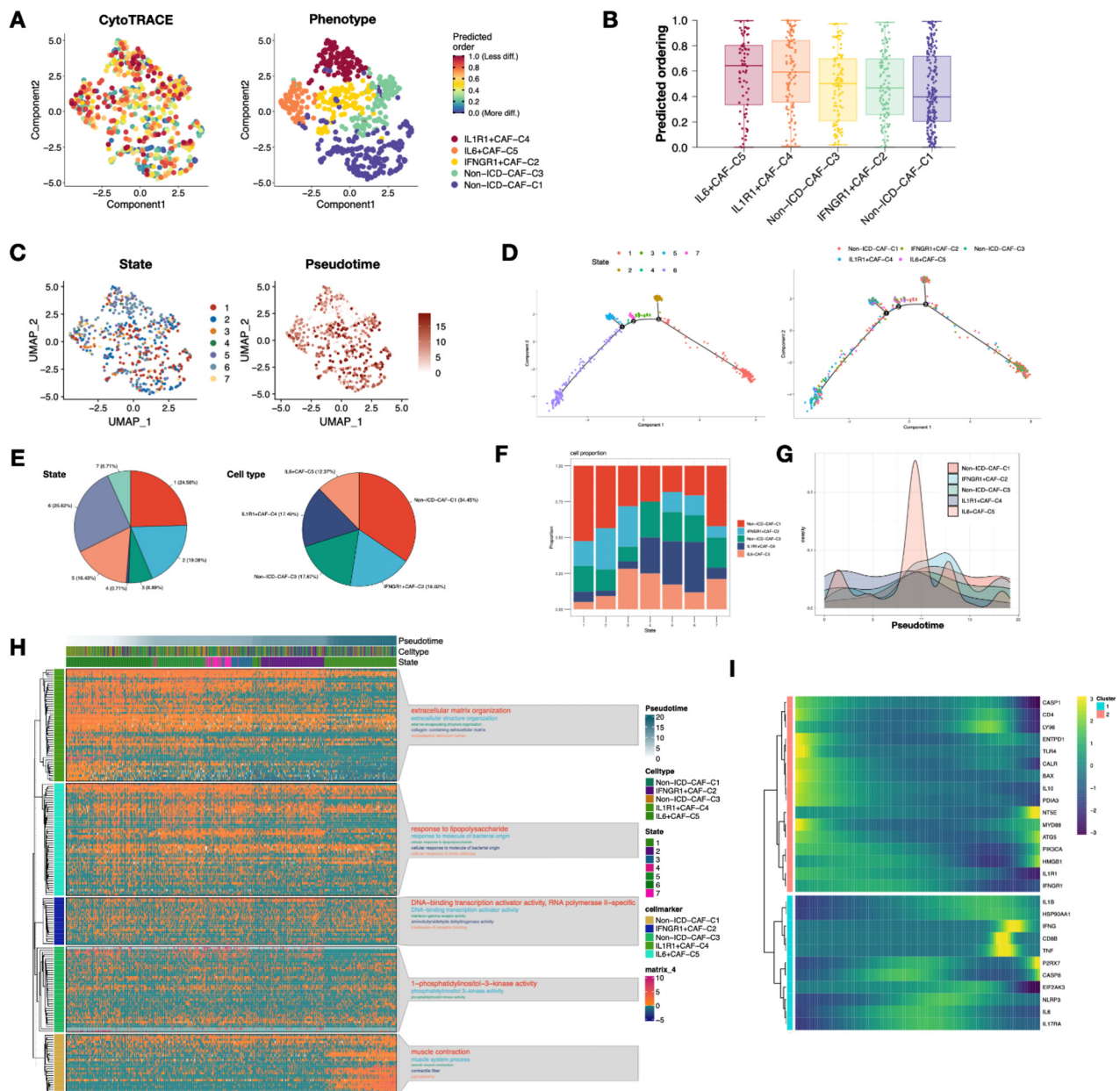
FIG. 2. Trajectory analysis of the CAF clusters. (a) CytoTRACE analysis showing the predicted order of the five CAF clusters. (b) CytoTRACE scores of the five CAF clusters. (c) Monocle analysis showing the predicted state and pseudotime of the five CAF clusters. (d) Trajectory analysis reveals CAF cluster development. (e, f) The cell proportion and state during the pseudotime of the five CAF clusters. (g) Ridge plot showing the pseudotime of each CAF cluster. (h) Heatmap showing the enrichment of marker genes from the five CAF clusters. (i) Trajectory analysis reveals the expression state of ICD-related genes.

results, the IFNGR1+CAF, IL6+CAF, and epithelial cells of the tumor all exhibited high MK signaling activity [Fig. 4(f)]. The two CAF clusters mostly acted as senders of MK signals in the network [Fig. 4(g)] to epithelial cells and other components [Fig. 4(h)]. The MDK-SDC1 ligand–receptor pair of the MK pathway was highly enriched in the CAF and tumor epithelial cell interaction [Fig. 4(i)], which was found involved in normal embryo epithelium development.[36]

## Risk model construction based on prognostic CAF clusters

675 DEGs of TCGA cohort showed a high correlation with prognostic CAF clusters (IFNGR1+CAF and IL6+CAF clusters) [supplementary material Fig. 2(a)], 23 of which were correlated with OS [supplementary material Fig. 2(b)]. LASSO-Cox analysis was performed [supplementary material Figs. 2(c) and 2(d)], and 9 genes were
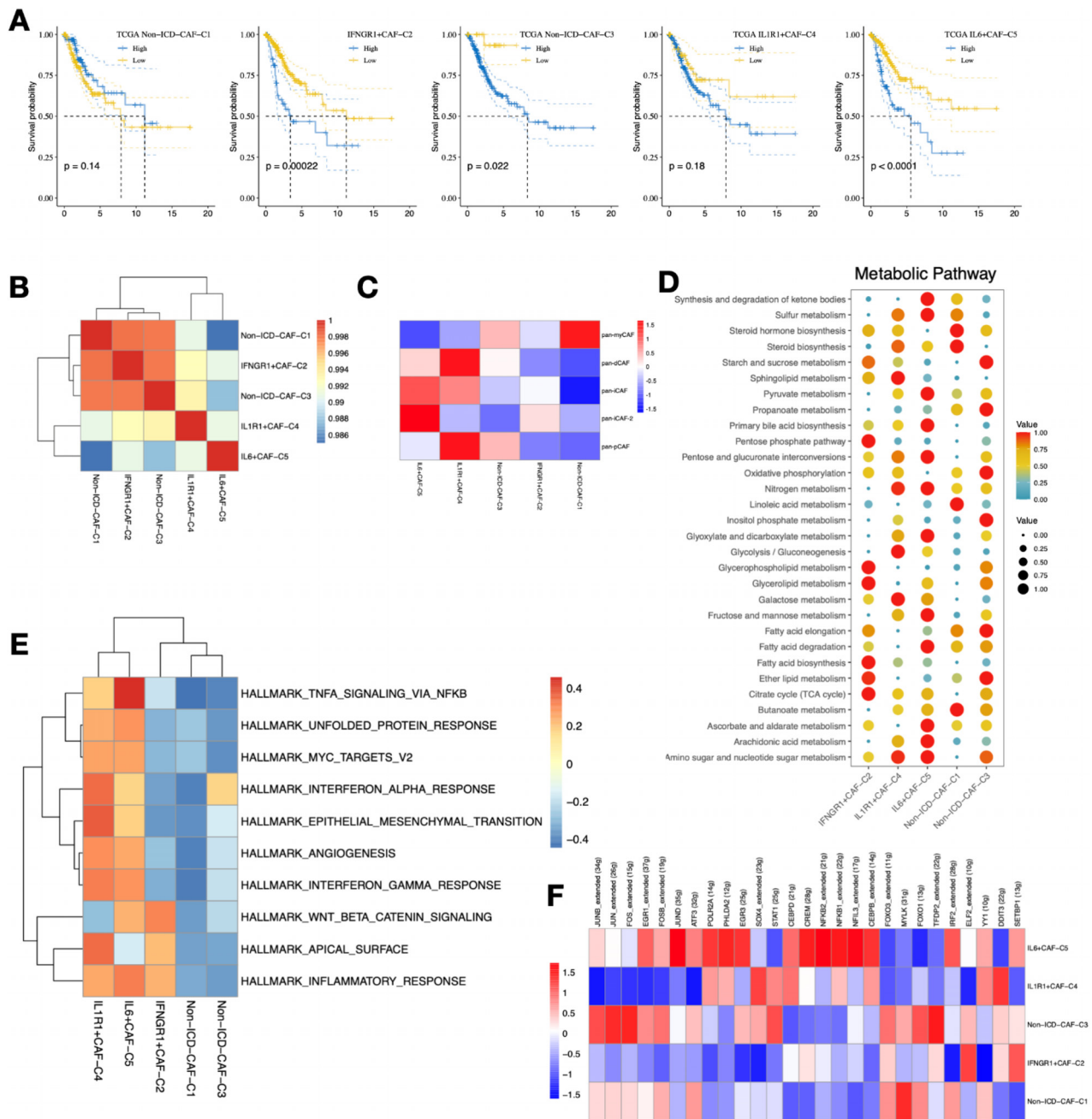
FIG. 3. Identification of prognostic value and functional characteristics of CAFs. (a) K–M plot of OS in high- and low-score groups of the five CAF clusters. Correlations between CAF clusters (b) and identified CAF signatures (c). (d) Heatmap showing metabolic signaling pathway activities. (e) Activated signaling ways and functions of the five CAF clusters. (f) Heatmap showing significantly different TFs among the five CAF clusters.

finally screened out. Then, the risk score was acquired by weighting hub gene expression with the regression coefficients [supplementary material Fig. 2(e)], after which patients were assigned to high-risk or low-risk groups based on the median risk score. Furthermore, individuals in the high-risk group had considerably poorer OS ($p < 0.0001$, log-rank test) and worse DSS ($p < 0.0001$, log-rank test)

[supplementary material Figs. 2(f) and 2(h)] than those in the low-risk group. Validation using GSE44001 of CC patients also demonstrated that the high-risk group had worse DFS than the low-risk group ($p = 0.0015$, log-rank test) [supplementary material Fig. 2(g)]. The ROC curve showed the AUC values are all above 0.70 in TCGA [supplementary material Fig. 2(i)]; and ranged from 0.57 to 0.65 in the
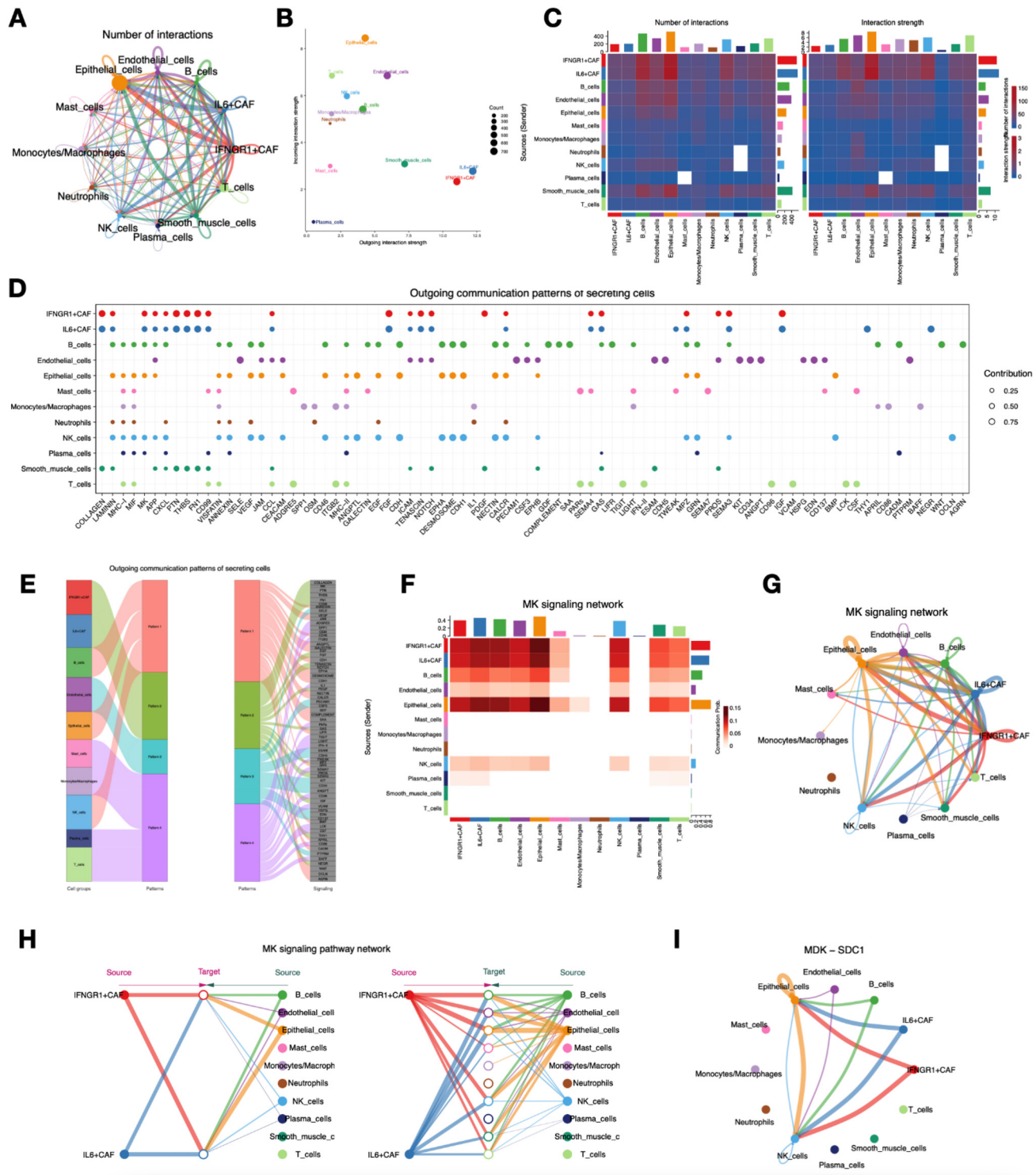
FIG. 4. Cell–cell communications of prognostic CAF clusters. (a) The interaction weight of the two prognostic CAF clusters and other cell types in tumor. (b) The relative level of incoming and outgoing strength of cell types in coordinate axes. (c) The correlation of incoming and outgoing strength between cell types. (d) Communication patterns of secreting cells. (e) Sankey plot of communication patterns. (f)–(h) MK signaling network analysis in CAF clusters. (i) The network showing the ligand–receptor pair of MDK-SDC1.
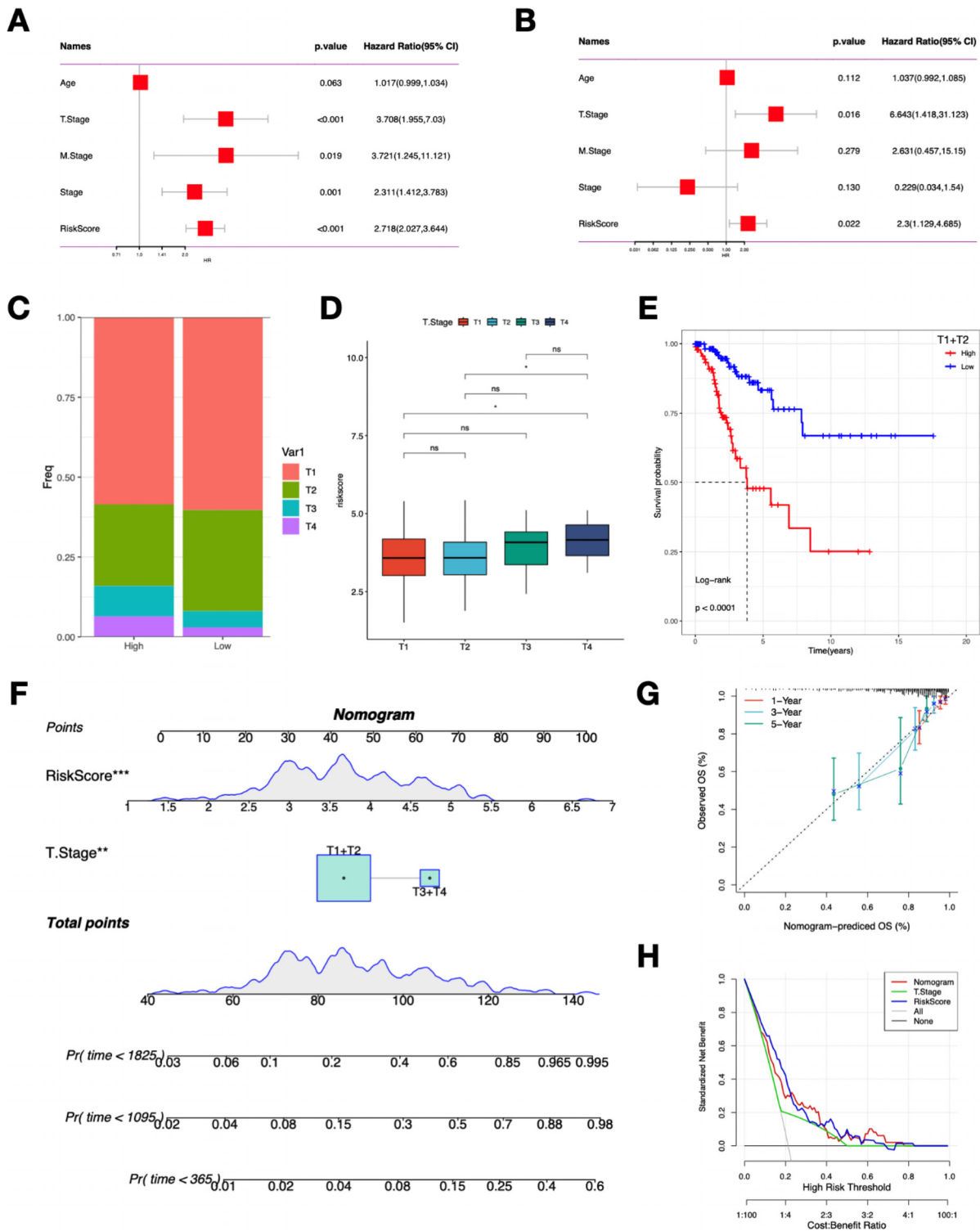
FIG. 5. Nomogram for CC prognosis prediction. Univariate Cox (a) and multivariate Cox (b) regression analysis of risk score. (c) The proportion of patients with different T stages in risk groups. (d) Comparison of the risk score among patients with different T stages. (e) Comparison of OS in high- and low-risk patients of T1 and T2. (f) Nomogram construction with the risk score and T stage. (g) Calibration curve prediction. (h) Decision curve for nomogram. ∗$P < 0.05$, ns, not significant.

validation GEO set [supplementary material Fig. 2(j)]. These findings demonstrated the risk model's strong discriminating capacity.

Clinical relationship of the risk model

Both univariate [Fig. 5(a)] and multivariate Cox [Fig. 5(b)] regression analyses demonstrated the risk score as an independent prognostic factor for CC ((HR > 1, p < 0.001). Additionally, we compared the risk score between patients with different T stages. The findings revealed that more patients of T3 and T4 were in the high-risk group [Fig. 5(c)]; patients with more advanced T stages had greater risk ratings compared to patients with less advanced T stages [Fig. 5(d)] and supplementary material, Fig. 3(a). Furthermore, using KM curve analysis, we discovered that high-risk patients in T1 and T2 had a much poorer prognosis (log-rank test, p < 0.0001) [Fig. 5(e)]. According to these results, the advanced tumor stage more likely occurred in patients with high risk. We created a nomogram based on the risk score and T stage to increase the clinical applicability [Fig. 5(f)]. The calibration curves were in good agreement with actual measurements and nomogram forecasts [Fig. 5(g)]. Furthermore, the C-index indicated the nomogram's consistent and strong predictive potential, outperforming other clinical features in OS prediction [supplementary material, Fig. 3(b)]. The DCA curve demonstrated that the nomogram exhibited superior net clinical benefit [Fig. 5(h)]. These results imply that the risk model provides a solid and accurate tool for customized prognosis prediction in CC patients.

Enrichment analysis for the risk model

The GSEA of the low-risk group was enriched in oxidative phosphorylation, E2F targets, and fatty acid metabolism [Fig. 6(a)]. The apical junction, coagulation, EMT, hypoxia, and inflammatory response were enriched in the high-risk group [Fig. 6(b)]. Furthermore, the high-risk group had higher activity in angiogenesis, TGF signaling, EMT, and hypoxia. The low-risk group had increased levels of oxidative phosphorylation, spermatogenesis, and fatty acid metabolism [Fig. 6(c)]. The risk model was strongly associated with metabolic pathways. Moreover, we performed KM curve analysis and found patients with higher scores of HALLMARKS_HYPOXIA, HALLMARK_CHOLESTEROL_HOMEOSTASIS, and HALLMARK_TGF_BETA_SIGNALING were associated with worse prognosis [Fig. 6(d)]. These findings imply that the various prognostic outcomes shown in the risk model may be influenced by the activation or inhibition of these pathways. Pathways, including oxidative phosphorylation, DNA replication, and endocytosis, were significantly correlated with the hub genes [Figs. 6(e) and 6(f)]. Further analysis of the risk score and risk genes may shed light on the mechanism underlining the pathology of CC.

Immune characteristics of the risk model

The immune-related pathways showed higher activity in the high-risk group [Fig. 7(a)]. The immune score and ESTIMATE score were negatively correlated with CFAP36, ERO1A, LDHA, SHF, and CENPM [Figs. 7(b) and 7(d)]. This suggests that higher expressions of these markers may contribute to an immunosuppressive tumor microenvironment, which is known to correlate with poorer immune responses and unfavorable clinical outcomes in CC patients. These findings underscore the potential of these biomarkers as indicators of

immune evasion mechanisms that could inform treatment strategies. In addition, the high-risk group had a lower abundance of activated CD8 T cells, and high proportion of CM CD4 T cells, and EM CD8 T cells [Fig. 7(c)]. The presence of these T cell subsets indicates an active immune response against the tumor, which may play a crucial role in controlling tumor progression. Specifically, activated CD8 T cells are essential for targeting and eliminating malignant cells, while CM CD4 T cells can facilitate robust immune responses through their ability to generate a pool of effector T cells. The higher abundance of EM CD8 T cells further suggests an ongoing adaptive immune response that might enhance anti-tumor activity. Furthermore, we discovered that the nine risk genes in the risk model were strongly associated with immune cells. C1orf74 showed a positive correlation with M1 macrophages, and CFAP36 and SHF were negatively correlated with M1 macrophages; ERO1A had a negative correlation with CD8 T cells [Fig. 7(e)]. Pearson's correlation analysis using the Mantel test revealed that immune cell types were substantially connected with risk score [Fig. 7(f)], including type 1 T helper cell, activated B cell, activated CD4 T cell, CM CD4 T cell, EM CD8 T cell, and activated dendritic cell.

Immunotherapy response of the risk model

The anticancer immune cycle was analyzed in risk groups. Patients with high and low risks demonstrated different steps of the anticancer immune cycle [supplementary material Fig. 4(a)]. In step 4, the low-risk group had a more remarkable ability for CD8 T cell recruitment [supplementary material Fig. 4(b)], indicating that there was a greater anticancer therapeutic response in the low-risk group. Higher immune checkpoint expression has been linked to a greater response to ICI therapy.[37–39] Thus, we examined the expression levels of immune checkpoints between risk groups. The immune checkpoints, such as CD27, PDCD1, LAG3, and TNFRSF18, were highly expressed in the low-risk group [supplementary material Fig. 4(c)]. To further validate our findings, we examined IPSs in risk groups. A better response to ICI treatment is predicted by higher IPSs. The low-risk group reacted more favorably to anti-PD-1 therapy than the high-risk group, with IPSs considerably higher for both CTLA4−/PD1− and CTLA4−/PD1+ therapies [supplementary material Fig. 4(d)]. Notably, the low-risk group exhibited a better OS in immunotherapy response in the IMvigor210 validation cohort [supplementary material Fig. 4(e)]. The group with low risk had a notably greater occurrence of individuals with progressing disease/stable disease (PD/SD) [supplementary material Fig. 4(f)] and a higher proportion of complete response/partial response (CR/PR) [supplementary material Fig. 4(g)]. In addition, low-risk patients of stage I/stage II and stage III/stage IV groups also showed better OS prediction [supplementary material Figs. 4(h) and 4(i)]. Furthermore, patients with melanomas in the GSE78220 cohort were also included for validation, and the low-risk patients exhibited better OS [supplementary material Fig. 4(j)], and patients of PR/CR were related to lower risk scores [supplementary material Figs. 4(k) and 4 (l)]. Therefore, immunotherapy may provide greater benefits to individuals classified as low-risk.

Identification of risk score in single-cell level

Cells of scRNA-seq data were regrouped into high- or low-risk groups based on hub gene expression [supplementary material Fig. 5

FIG. 6. Enrichment analysis of risk score and hub genes. (a) Ridge plot showing the GO terms in the low-risk group. (b) GSEA analysis of the high-risk group. (c) Hallmark pathway activities between risk groups. (d) Correlations between the risk score and pathway activities. (e) and (f) Heatmap showing the correlation between hub genes and related pathways.

FIG. 7. The immune features associated with risk score and hub genes in CC. (a) Immune-related pathway in risk groups. (b) Heatmap showing the correlation between hub genes and stromal score, immune score, and ESTIMATE score. (c) Landscape of immune cells in high- and low-risk groups. (d) The correlation between hub genes and immune scores. (e) Heatmap showing the correlation between hub genes and TICs. (f) Mantel test of correlation between risk score and TICs. ∗P < 0.05, ∗∗P < 0.05, ∗∗∗P < 0.001, ns, not significant.

(a)]. Within the risk groups, the distribution of cell types was examined [supplementary material Fig. 5(b)], revealing a higher abundance of T cells in the low-risk group. The distribution of the nine risk genes is illustrated in the supplementary material, Fig. 5(c), and we found that the high-risk cells had significant amounts of MCAM and LDHA. Enrichment analysis demonstrated that the cholesterol homeostasis, hypoxia, and p53 pathway were correlated with the high-risk cells [supplementary material Fig. 5(d)]. The DEGs of high- and low-risk cells were enriched in fluid shear stress and atherosclerosis, focal adhesion, and proteoglycans in cancer [supplementary material Fig. 5(e)]. Then, we combined the risk score, ICD score, and top DEGs of the high- and low-risk cells to illustrate their correlations in the scRNA-seq analysis [supplementary material Fig. 5(f)]. ERO1A was elevated in the high-risk cells, mainly in epithelial cells of the tumor group. Subsequently, we distinguished tumor epithelial cells with high and low risk levels and examined their interactions with other kinds of cells (supplementary material, Fig. 6). We examined the interaction between high-risk epithelial cells and fibroblasts, NK cells, and T cells. The results showed that the high-risk epithelial cells communicate with the three cell types through various pathways and ligand pairs, including MIF, APP, and MDK signaling pathways [supplementary material Fig. 5(g)].

Drug sensitivity analysis and hub gene validation

Based on the risk score, we found that bosutinib and bexarotene were sensitive to the high-risk patients; Etoposide and tipifarnib were sensitive to the low-risk patients [supplementary material Fig. 7(a)]. Furthermore, we validated the nine hub genes within HaCaT, HeLa, and SiHa. We found that SHF and PEAR1 were significantly downregulated in the SiHa cells, and CFAP36 were significantly downregulated, whereas CENPM, C1orf74, and ERO1A were significantly upregulated in the HeLa cells [supplementary material Fig. 7(b)]. Finally, we performed IHC of IL6, IFNGR1, and ERO1A in CC samples. We found that IL6 and IFNGR1 were mainly distributed in the stromal component of CC tissue. Besides, the ERO1A was found upregulated compared to normal tissue and distributed in the epithelium and glands [supplementary material Fig. 7(c)].

DISCUSSION

Based on scRNA-seq, specific subclusters of CAFs and the mechanism of CAFs contributing to tumor progress in cervical cancer have been identified. However, the tumorigenic effect of ICD-modified CAF clusters remains elusive. In this work, we used the NMF approach to conduct multi-omics investigations on the variety of CAFs based on ICD-related genes. The significant advantage of our CAF classification is that we screened out the specific CAF clusters affected by the ICD patterns and identified cell interactions in the TME. CAFs significantly influence tumor progression and immune modulation, making them vital targets for therapeutic strategies aimed at enhancing anti-tumor immunity. This unique and innovative perspective has allowed us to comprehend the impact of CAF clusters, which are influenced by ICD-related alterations in the TME, on the prognosis of individual CC patients.

The study found that the IL6+CAF and IFNGR1+CAF led to worse prognoses in CC patients. CAFs have been implicated in chemotherapy resistance and metastasis by releasing factors into the TME. We further analyzed the characteristics of IL6+CAF and IFNGR1+CAF clusters in metabolic pathways, TF networks, and the communication between other cell types of CC. The IL6+CAF exhibited high NFKB regulator activity, which was found related to CC progression.[40] The activation of NFKB influences the innate and adaptive immune responses of CC progression.[41] NFKB becomes inherently engaged throughout the progression of high-grade intraepithelial neoplasia and CC, and inhibiting the NFKB signaling pathway effectively limits cervical tumor cell development.[42] NFKB may induce transcription of proliferation-regulating genes, metastasis-related genes, and telomerase-mediated cell immortality.[43] The IFNGR1+CAF showed aberrant lipid metabolism pathway, and the lipid metabolism is a critical characteristic of cancer cells.[44] During the proliferation process, lipid synthesis supplies a crucial substrate for energy metabolism as well as components for cell membrane building, implying that lipid metabolism pathways play an important role in the genesis and progression of cancer.[45,46] The prognostic IFNGR1+CAF's regulation of lipid metabolism may provide a reference for selecting treatment strategies in CC patients.

The crosstalk between CAF and cancer cells modulates cancer metastasis and therapeutic resistance.[47] From cell chat analysis, the IL6+CAF and IFNGR1+CAF exhibited the most potent interaction with the epithelial cells and extreme outgoing patterns distinct from other cell types. Furthermore, we found the MK signaling network of the CAF clusters that strongly interacted with tumor epithelial cells in CC. The MK pathway was recognized as an emerging oncoprotein and mesenchymal transition (EMT) inducer[48] and was found elevated in CC.[49] The activation of EMT led to tumor progression, metastasis, and recurrence of CC. Therapeutic strategies focused on EMT suppression ameliorate cervical cancer pathogenesis.[50] Hu *et al.* found that MK and SDC1 correlate with the malignant progression.[51] In our study, the MK–SDC1 pair also demonstrated high interactions from IL6+CAF and IFNGR1+CAF to epithelial cells in tumor, further proving their role in tumor formation.

Molecular biomarkers and signatures benefit preclinical and clinical cancer therapies. We created a ICD-related CAF-based risk model with nine hub genes. The risk scores that link the immunology and prognosis of CC were identified. A nomogram was created, and the area under ROC curves for OS prediction of one, three, and five years was more than 0.7, demonstrating the risk model's exceptional prediction capacity in CC.

To understand the biological pathways underpinning the risk model, we used multi-omics methods. We discovered that hypoxia and TGF were concentrated in high-risk patients, and a high score of hypoxia/TGF correlates with a worse OS. Low tumorous oxygenation raises the probability of local invasion, metastasis, and treatment failure in the etiology of CC.[52] A hypoxic tumor stroma may promote tumor cell stemness and accelerate tumor development by increasing CAF secretion. Hypoxia induces the activation of NFKB pathway in CC and facilitates tumor migration and invasion.[53] The positive correlation of the risk score and hypoxia activity may contribute to CC pathology. Li *et al.* found the blockade of TGFβ enhances chemotherapy,[54] which also gives a strategy for anticancer therapy.

Furthermore, the risk score showed a more vital independent prognostic ability than other clinicopathologic features. The low-risk group exhibited increased immune checkpoints, indicating that immune checkpoint inhibitors may be a viable alternative for low-risk individuals. Furthermore, our findings demonstrated that the CAF-

based risk model might predict response to anti-PD-L1 immunotherapy. Aside from immunotherapy, we also investigated the IC50 of medication sensitivity, and the sensitive drugs for patients of high risk were identified. Combining immunogenic therapy and innovative immunotherapeutic regimens for treating CC shows considerable potential. Taking the risk score into account may help with the personalized treatment of CC patients. Overall, these results provide potential therapeutic options for CC.

We validated the ERO1A both in CC cells and tissues and found it elevated in CC, consistent with previous studies.[55,56] The ERO1A has a role in tumor metastasis and EMT through Wnt, mTOR, and VEGF pathways.[55] Liu *et al.* found the ablation of ERO1A induces ICD to activate anti-tumor immunity,[57] and upregulation of ERO1A may arise in the recruitment of immune-suppressive cells, resulting in an immune-suppressive TME.[58] Thus, targeting ERO1A may offer alternative therapeutic strategies for CC.

Nonetheless, several shortcomings should be addressed. First, this is a retrospective data analysis, and it must be validated in multi-center CC cohorts. Second, we mainly investigated the CAF-based risk model's potential predictive relevance; consequently, to confirm the underlying processes of the risk model in CC, further research is necessary.

CONCLUSION

Table I outlines the main findings and emphasizes the significance of CAF subtypes and the developed risk model in understanding cancer progression and guiding treatment. The results indicate that tumor fibroblasts exhibit higher ICD scores than normal ones, with significant CAF subtypes (e.g., IFNGR1+CAF, IL6+CAF, and ILR1+CAF) identified as key players in tumor progression. Pseudotime analysis revealed less differentiated CAFs such as IL6+CAF and ILR1+CAF, positioned at the start of the developmental process. IFNGR1+CAF and IL6+CAF were associated with worse OS, and enrichment analysis highlighted their involvement in immune signaling pathways. Cell–cell interaction analysis underscored pathways like MDK-SDC1 between CAFs and epithelial cells, signifying active tumor–environment communication. A nine-gene risk model was constructed, showing its prognostic independence and correlation with worse OS and increased immune checkpoint expression in low-risk patients. High-risk groups displayed enrichment in EMT, hypoxia, and angiogenesis, while low-risk patients had better immune responses and higher immune cell infiltration, suggesting improved responses to ICIs. This risk model may serve as an independent predictor of prognosis and help with treatment strategies.

METHODS

Data processing

RNA sequencing files (fragments per kilobase of exon model per million mapped fragments, FPKM) for the TCGA-CESC cohort were obtained. Clinical information was extracted. Patients who lacked clinical information were eliminated from further analysis. The GSE44001 cohort with gene expression and survival data of 300 CC patients were obtained from the Gene Expression Omnibus (GEO) database. Additionally, we acquired the CC scRNA-seq dataset E-MTAB-12350 from the ArrayExpress database. For predicting immune response, the IMvigor210 cohort[59] with patients receiving atezolizumab and the GSE78220 cohort of pretreatment melanomas undergoing checkpoint inhibition therapy were retrieved. From previously published research,

32 ICD-related genes (supplementary material, Table I) were determined.[60,61]

Single-cell RNA-seq analysis and CAF cluster identification

With the "Seurat" package,[62] cells with mitochondrial genes less than 15% were collected. The top 2000 highly variable genes were identified for the data scale. The data from the seven samples were cleaned of batch effects using the "Harmony" package.[63] Cell clusters were identified using the "FindClusters" and "FindNeighbors" functions. The cell types were first recognized using the "SingleR" package[64] and then annotated manually with marker genes from the CellMarker database[65] and previous paper.[19] The FindAllMarkers tool was used to detect marker genes in each cell cluster that exhibited a log fold change more than 0.35, a minimum percentage greater than 0.35, and an adjusted p-value less than 0.05. The non-negative matrix factorization (NMF) in R was used to identify clusters of CAFs related to ICD. To display the top gene expression levels in each NMF cluster, the Dotplot tool was used.

Identification of risk genes correlated with the prognostic CAF clusters

DEGs were screened with FDR < 0.001 and logFC > 1. Then, using p < 0.001 and cor > 0.4, prognostic DEGs correlated with prognostic CAF clusters were examined. Then, LASSO analysis was used for hub gene selection. We created a risk model after the multivariate Cox calculation: risk score $= \beta$i EXP) (EXP: expression level; βi reflects the coefficient in the multivariate Cox model). After zero-mean normalization, the patients were separated into high- and low-risk groups. To assess the prediction performance of the risk model, the "timeROC" package was used. In the validation cohort, the same studies were carried out.

Pseudotime trajectory analysis of ICD-related genes for CAF clusters

To study the pseudotime trajectories of CAF clusters, the "cytoTRACE" and "Monocle2" package was used.[66] The DDRTree technique was used for the purpose of reducing dimensionality. Next, we used the "plot_pseudotime_heatmap" method to generate heatmaps that depict the changing expression patterns of genes associated with ICD in the pseudotime trajectories.

Cell communication analysis for CAF clusters

The "CellChat" package offers ligand–receptor interaction databases to examine intercellular communication networks within cell clusters.[67] Initially, we used CellChatDB.human to evaluate the primary signaling inputs and outputs in all CAF clusters. Subsequently, we constructed cell–cell communication networks connecting the target cell cluster with the CAF clusters. The netVisual bubble function creates bubble charts that illustrate important interactions between cell clusters including ligands and receptors.

TABLE I. Summary of key results from the analysis.

Analysis type	Subheading	Key findings
Identification and characterization	Cell types and ICD scores	11 major cell types identified, including T cells, monocytes/macrophages, fibroblasts, NK cells; higher ICD scores in T cells, monocytes/macrophages, and mast cells.
	Tumor vs. normal fibroblasts	Elevated ICD scores in fibroblasts in tumor samples compared to normal.
	CAF subclusters	Five clusters identified: Non-ICD-CAF-C1, IFNGR1+CAF-C2, Non-ICD-CAF-C3, ILR1+CAF-C4, IL6+CAF-C5.
	Key ICD genes	IFNGR1, ILR1, IL6 identified as key genes.
Pseudotime trajectory analysis	CytoTRACE and monocle analysis	IL6+CAF and ILR1+CAF show higher CytoTRACE scores (less differentiated); monocle analysis shows IL6+CAF and ILR1+CAF at starting point.
	Gene activation	ENTPD1, TLR4, MYD88 active early; NT5E, P2RX7 active later.
Prognostic and functional analysis	Survival analysis	IFNGR1+CAF and IL6+CAF linked to worse survival.
	Functional characteristics	IL6+CAF linked to iCAF; IL1R1+CAF to dCAF/pCAF.
	Pathway associations	IL6+CAF associated with TNFA_SIGNALING_VIA_NFKB; IFNGR1+CAF associated with energy production pathways.
Cell–cell interaction analysis	Interaction networks	IFNGR1+CAF and IL6+CAF have strong interactions with epithelial cells.
	Key pathways	Enrichment in COLLAGEN, PTN, MK signaling.
	Ligand–receptor Pair	MDK-SDC1 pair enriched in CAF–epithelial cell interaction.
Risk model and validation	Prognostic DEGs and model	675 CAF-associated DEGs identified, 23 linked to OS; LASSO-Cox model with 9 hub genes.
	Risk group outcomes	High-risk group had poorer OS and DSS; validated with ROC AUC > 0.70 in TCGA dataset, 0.57–0.65 in GEO dataset.
Clinical relevance	Independent prognostic factors	Risk score shown as independent prognostic factor (HR > 1, p < 0.001).
	Tumor stage correlation	High-risk group predominantly in T3 and T4 stages.
	Nomogram development	Strong predictive accuracy and calibration with clinical outcomes.
Enrichment and immune characteristics	GSEA and immune pathways	High-risk group enriched in EMT, hypoxia, angiogenesis; higher immune pathway activity.
	Immune cell correlations	High-risk group linked to activated CD8 T cells, EM CD8 T cells, etc.
Immunotherapy response	Immune cycle and checkpoints	Low-risk group had better CD8 T cell recruitment; higher expression of CD27, PDCD1, LAG3, TNFRSF18.
	IPSs	Higher IPSs in low-risk group, predicting better ICI therapy response.

Functional enrichment analysis for CAF clusters

The R package "clusterProfiler" was used to identify the Kyoto Encyclopedia of Genes and Genomes (KEGG). The ssGSEA score was used to identify prospective paths for risk modeling. We calculated the GSVA ratings for 50 significant pathways. The c5.go.v7.5.1.symbols.gmt file was used in the GSEA analysis to determine enrichment.

SCENIC analysis for ICD-related CAF clusters

Co-expression and DNA motif analysis were used to construct the gene regulatory network by the "SCENIC" package.[68] Key transcription factors (TFs) were identified. The gene-motif ranking, namely, the hg19-tss-centered-10 kb and hg19-500 bp-upstream, were used as references.

Survival analysis and nomogram construction

The "survminer" package was used for the OS, progression-free survival (PFS), and disease-specific survival (DSS) analyses between risk groups. To discover whether the risk score was a reliable predictor of CC patients' survival, univariate and multivariate Cox regression analyses were conducted. A nomogram that incorporated the risk score and T stages was established for survival prediction. Finally, the

nomogram's precision was assessed using calibration curves and decision curve analysis (DCA).

Immune characteristics of the risk model

We used "CIBERSORT" package to quantify immune cell infiltrating and the ESTIMATE algorithm to examine the association between risk score and immune cell infiltration. For TCGA-CESC samples, we used the Tracking Tumor Immunophenotype platform to get activity scores for each of the seven anticancer immune processes. The Immunophenotypescore (IPS) corresponds with tumor immunogenicity as an ICI response predictor; a high IPS suggests an effective response to ICI treatment. The CESC cohort's IPS was obtained from The Cancer Immunome Atlas database.

Drug sensitivity analysis

We used the "pRRophetic" package to compare the half-maximal inhibitory concentration (IC50) of medicines across risk groups, using a p-value of less than 0.05 for the Wilcoxon test.

Quantitative real-time polymerase chain reaction (qRT-PCR)

Total RNA was isolated from two CC cell lines, namely, HeLa and SiHa, as well as human keratinocytes of HaCaT cells as control. Total RNA extractions were performed using Trizol reagent. Total RNA was reverse transcribed using the M-MLV-RT system (Promega, USA). qPCR was conducted using SYBR PCR mix reagent (RR430A, Takara, China) according to instructions. The primers used are demonstrated in the supplementary material, Table II.

Immunohistochemistry

Immunohistochemistry (IHC) was used to validate key genes in CC tissue collected from the Second Hospital of Jilin University. The ethics council of the Second Hospital of Jilin University accepted the study (NO: 2022029). The paraffin-embedded CC tissues were IHC stained after dewaxing and rehydration. The slices were subjected to overnight treatment at a temperature of $4\,^{\circ}$C with primary antibodies, including IL6 (1:100, Abclonal, A0286, China), IFNGR1 (1:100, Abclonal, A21912, China), and ERO1A (1:200, Abcam, ab177156, USA) followed by biotinylated goat anti-rabbit IgG secondary antibody and were visualized using diaminobenzidine tetrachloride (DAB) staining.

Statistical analysis

To examine the variations in clinical features between the risk groups, the chi-squared test was employed. Correlation between the risk score and immune cell infiltration was investigated using Pearson's correlation analysis. ANOVA was used to examine the qRT-PCR data. Statistical significance was set at $p < 0.05$.

SUPPLEMENTARY MATERIAL

See the supplementary material for the following: Supplementary Table I for details on primers used for hub gene validation; Supplementary Table II for details on ICD-related genes; Supplementary Table III for details on marker genes of CAF clusters; Supplementary Fig. 1 for illustration of scRNA-seq analysis of CC dataset—PCA plot before (a) and after (b) harmony, (c) 26 clusters demonstrated by tSNE, (d) ICD score of normal and tumor samples, (e) top 5 marker genes of the five CAF clusters, and (f) UMAP plot of the expression of IFNGR1, IL1R1, and IL6 in scRNA-seq dataset; Supplementary FIG. 2 for illustration of hub gene selection and risk model construction—(a) volcano plot of DEGs in TCGA-CESC cohort, (b) prognostic DEGs identification, (c) distribution of variable lambda, (d) plots showing coefficient distributions, (e) the coefficients for each risk gene in the model, KM curves for OS in TCGA cohort (f), for DFS in GSE44001 cohort (g), and for DSS in TCGA cohort (h), ROC curves of the TCGA cohort (i) and GSE44001 cohort (j); Supplementary Fig. 3 for illustration of clinical features in the risk model—(a) comparison of risk score between patients of T1-2 and T3-4 and (b) C-index analysis; Supplementary Fig. 4 for illustration of immunotherapy prediction of the risk model—(a) immunity cycle activity of risk groups, (b) radar plot showing different recruited immune cells, (c) immune checkpoint detection, (d) the IPS between risk groups, (e) OS prediction of IMvigor210 cohort, (f) risk scores of immunotherapy responses in the IMvigor210 cohort, (g) the prediction of CR/PR or SD/PD of the IMvigor210 cohort, prediction of OS in patients at an early stage (h) and advanced stage (i) in the IMvigor210 cohort, (j) OS prediction of the GSE78220 cohort, the prediction of immunotherapy responses (k) and evaluation of tumor therapy (l) in the GSE78220 cohort, $*P < 0.05$, $**P < 0.05$, $***P < 0.001$, $****P < 0.0001$; Supplementary Fig. 5 for illustration of the correlation of risk score with single-cell characteristics—(a) the distribution of high- and low-risk cells, (b) the distribution of cell types among different risk categories, (c) tSNE plot of hub gene distribution, GSEA analysis (d) and KEGG analysis (e) of the risk cells, (f) heatmap showing hub genes in different cell types, risk groups, and ICD score groups, and (g) the ligand–receptor interactions networks; Supplementary Fig. 6 for illustration of the communication of high- and low-risk epithelial cells in scRNA-seq dataset; and Supplementary Fig. 7 for illustration of the association between risk score and drug sensitivity and gene validation—(a) sensitive drugs for high- and low-risk patients, (b) validation of the expression of the nine hub genes by qRT-PCR, (c) IHC of IL6, IFNGR1, and ERO1A in CC tissues, $*P < 0.05$, $***P < 0.001$, ns, not significant.

AUTHOR DECLARATIONS

Conflict of Interest

The authors have no conflicts to disclose.

Ethics Approval

Ethics approval is not required.

Author Contributions

Fei Wu: Conceptualization (equal); Data curation (equal); Formal analysis (equal); Funding acquisition (equal); Investigation (equal); Methodology (equal); Project administration (equal); Writing – original draft (equal); Writing – review & editing (equal). **Yue Xu:** Conceptualization (equal); Data curation (equal); Formal analysis (equal); Funding acquisition (equal); Investigation (equal); Methodology (equal); Project administration (equal); Resources (equal); Validation (equal); Visualization (equal); Writing – original draft (equal); Writing – review & editing (equal).

DATA AVAILABILITY

The data that support the findings of this study are available from the corresponding author upon reasonable request.

NOMENCLATURE

AUC	Area under the curve
CAFs	Cancer-associated fibroblasts
CC	Cervical cancer
EMT	Epithelial-mesenchymal transition
ERO1A	Endoplasmic reticulum oxidoreductase 1 alpha
HPV	Human papillomavirus
ICD	Immunogenic cell death
iCAFs	Inflammatory cancer-associated fibroblasts
IFNGR1	Interferon gamma receptor 1
IL6	Interleukin 6
mTOR	mechanistic target of rapamycin
myCAFs	Pro-tumorigenic cancer-associated myofibroblasts
NFKB	Nuclear Factor Kappa-Light-Chain-Enhancer of Activated B Cells
OS	Overall survival
SDC1	Syndecan 1
TGF	Transforming growth factor
TME	Tumor microenvironment
VEGF	Vascular endothelial growth factor

REFERENCES

[1]A. Fernandes, D. Viveros-Carreño, J. Hoegl, M. Ávila, and R. Pareja, "Human papillomavirus-independent cervical cancer," Int. J. Gynecol. Cancer 32(1), 1–7 (2022).

[2]W. Small, M. A. Bacon, A. Bajaj, L. T. Chuang, B. J. Fisher, M. M. Harkenrider, A. Jhingran, H. C. Kitchener, L. R. Mileshkin, A. N. Viswanathan, and D. K. Gaffney, "Cervical cancer: A global health crisis," Cancer 123(13), 2404–2412 (2017).

[3]H. Sung, J. Ferlay, R. L. Siegel, M. Laversanne, I. Soerjomataram, A. Jemal, and F. Bray, "Global Cancer Statistics 2020: GLOBOCAN Estimates of Incidence and Mortality Worldwide for 36 Cancers in 185 Countries," CA. A Cancer J. Clin. 71(3), 209–249 (2021).

[4]Y. Yuan, X. Cai, F. Shen, and F. Ma, "HPV post-infection microenvironment and cervical cancer," Cancer Lett. 497, 243–254 (2021).

[5]C. Güzel, J. van Sten-Van't Hoff, I. M. C. M. de Kok, N. I. Govorukhina, A. Boychenko, T. M. Luider, and R. Bischoff, "Molecular markers for cervical cancer screening," Expert Rev. Proteomics 18(8), 675–691 (2021).

[6]L. V. Volkova, A. I. Pashov, and N. N. Omelchuk, "Cervical carcinoma: Oncobiology and biomarkers," Int. J. Mol. Sci. 22(22), 12571 (2021).

[7]H. B. Musunuru, P. M. Pifer, P. Mohindra, K. Albuquerque, and S. Beriwal, "Advances in management of locally advanced cervical cancer," Indian J. Med. Res. 154(2), 248–261 (2021).

[8]P. F. Cosper, C. McNair, I. González, N. Wong, K. E. Knudsen, J. J. Chen, S. Markovina, J. K. Schwarz, P. W. Grigsby, and X. Wang, "Decreased local immune response and retained HPV gene expression during chemoradiotherapy are associated with treatment resistance and death from cervical cancer," Int. J. Cancer 146(7), 2047–2058 (2020).

[9]M. Narasimhamurthy and S. U. Kafle, "Cervical cancer in Nepal: Current screening strategies and challenges," Front. Public Health 10, 980899 (2022).

[10]S. Zhu, Y. Wang, J. Tang, and M. Cao, "Radiotherapy induced immunogenic cell death by remodeling tumor immune microenvironment," Front. Immunol. 13, 1074477 (2022).

[11]Z. Li, X. Lai, S. Fu, L. Ren, H. Cai, H. Zhang, Z. Gu, X. Ma, and K. Luo, "Immunogenic cell death activates the tumor immune microenvironment to boost the immunotherapy efficiency," Adv. Sci. 9(22), e2201734 (2022).

[12]J. Zhou, G. Wang, Y. Chen, H. Wang, Y. Hua, and Z. Cai, "Immunogenic cell death in cancer therapy: Present and emerging inducers," J. Cell. Mol. Med. 23(8), 4854–4865 (2019).

[13]P. Liu, L. Zhao, J. Pol, S. Levesque, A. Petrazzuolo, C. Pfirschke, C. Engblom, S. Rickelt, T. Yamazaki, K. Iribarren, L. Senovilla, L. Bezu, E. Vacchelli, V. Sica, A. Melis, T. Martin, L. Xia, H. Yang, Q. Li, J. Chen, S. Durand, F. Aprahamian, D. Lefevre, S. Broutin, A. Paci, A. Bongers, V. Minard-Colin, E. Tartour, L. Zitvogel, L. Apetoh, Y. Ma, M. J. Pittet, O. Kepp, and G. Kroemer, "Crizotinib-induced immunogenic cell death in non-small cell lung cancer," Nat. Commun. 10(1), 1486 (2019).

[14]P.-J. Wu, H.-L. Chiou, Y.-H. Hsieh, C.-L. Lin, H.-L. Lee, I.-C. Liu, and T.-H. Ying, "Induction of immunogenic cell death effect of licoricidin in cervical cancer cells by enhancing endoplasmic reticulum stress-mediated high mobility group box 1 expression," Environ. Toxicol. 38(7), 1641–1650 (2023).

[15]Z. Li, C. Sun, and Z. Qin, "Metabolic reprogramming of cancer-associated fibroblasts and its effect on cancer cell reprogramming," Theranostics 11(17), 8322–8336 (2021).

[16]Z. Liao, Z. W. Tan, P. Zhu, and N. S. Tan, "Cancer-associated fibroblasts in tumor microenvironment—Accomplices in tumor malignancy," Cell Immunol. 343, 103729 (2019).

[17]N. Erez, M. Truitt, P. Olson, S. T. Arron, and D. Hanahan, "Cancer-associated fibroblasts are activated in incipient neoplasia to orchestrate tumor-promoting inflammation in an NF-kappaB-dependent manner," Cancer Cell 17(2), 135–147 (2010).

[18]T. Murata, E. Mekada, and R. M. Hoffman, "Reconstitution of a metastatic-resistant tumor microenvironment with cancer-associated fibroblasts enables metastasis," Cell Cycle 16(6), 533–535 (2017).

[19]C. Li, D. Liu, S. Yang, and K. Hua, "Integrated single-cell transcriptome analysis of the tumor ecosystems underlying cervical cancer metastasis," Front. Immunol. 13, 966291 (2022).

[20]Z. Ou, S. Lin, J. Qiu, W. Ding, P. Ren, D. Chen, J. Wang, Y. Tong, D. Wu, A. Chen, Y. Deng, M. Cheng, T. Peng, H. Lu, H. Yang, J. Wang, X. Jin, D. Ma, X. Xu, Y. Wang, J. Li, and P. Wu, "Single-nucleus RNA sequencing and spatial transcriptomics reveal the immunological microenvironment of cervical squamous cell carcinoma," Adv. Sci. 9(29), e2203040 (2022).

[21]C. Li, H. Wu, L. Guo, D. Liu, S. Yang, S. Li, and K. Hua, "Single-cell transcriptomics reveals cellular heterogeneity and molecular stratification of cervical cancer," Commun. Biol. 5(1), 1208 (2022).

[22]Y. Sheng, B. Zhang, B. Xing, Z. Liu, Y. Chang, G. Wu, and Y. Zhao, "Cancer-associated fibroblasts exposed to high-dose ionizing radiation promote M2 polarization of macrophages, which induce radiosensitivity in cervical cancer," Cancers 15(5), 1620 (2023).

[23]G. J. Yoshida, "Regulation of heterogeneous cancer-associated fibroblasts: The molecular pathology of activated signaling pathways," J. Exp. Clin. Cancer Res. 39(1), 112 (2020).

[24]X. Mao, J. Xu, W. Wang, C. Liang, J. Hua, J. Liu, B. Zhang, Q. Meng, X. Yu, and S. Shi, "Crosstalk between cancer-associated fibroblasts and immune cells in the tumor microenvironment: New findings and future perspectives," Mol. Cancer 20(1), 131 (2021).

[25]T. Kordaß, W. Osen, and S. B. Eichmüller, "Controlling the immune suppressor: Transcription factors and microRNAs regulating CD73/NT5E," Front. Immunol. 9, 813 (2018).

[26]F. Di Virgilio, D. Dal Ben, A. C. Sarti, A. L. Giuliani, and S. Falzoni, "The P2X7 receptor in infection and inflammation," Immunity 47(1), 15–31 (2017).

[27]P. M. Galbo, X. Zang, and D. Zheng, "Molecular features of cancer-associated fibroblast subtypes and their implication on cancer pathogenesis, prognosis, and immunotherapy resistance," Clinical Cancer Res. 27(9), 2636–2647 (2021).

[28]X. Pan, J. Zhou, Q. Xiao, K. Fujiwara, M. Zhang, G. Mo, W. Gong, and L. Zheng, "Cancer-associated fibroblast heterogeneity is associated with organ-specific metastasis in pancreatic ductal adenocarcinoma," J. Hematol. Oncol. 14(1), 184 (2021).

[29]Y. Gao, H. Wang, S. Chen, R. An, Y. Chu, G. Li, Y. Wang, X. Xie, and J. Zhang, "Single-cell N6-methyladenosine regulator patterns guide intercellular communication of tumor microenvironment that contribute to colorectal cancer progression and immunotherapy," J. Transl. Med. 20(1), 197 (2022).

[30]G. Friedman, O. Levi-Galibov, E. David, C. Bornstein, A. Giladi, M. Dadiani, A. Mayo, C. Halperin, M. Pevsner-Fischer, H. Lavon, S. Mayer, R. Nevo, Y.

Stein, N. Balint-Lahat, I. Barshack, H. R. Ali, C. Caldas, E. Nili-Gal-Yam, U. Alon, I. Amit, and R. Scherz-Shouval, "Cancer-associated fibroblast compositions change with breast cancer progression linking the ratio of S100A4+ and PDPN+ CAFs to clinical outcome," Nat. Cancer **1**(7), 692–708 (2020).

[31]A. Costa, Y. Kieffer, A. Scholer-Dahirel, F. Pelon, B. Bourachot, M. Cardon, P. Sirven, I. Magagna, L. Fuhrmann, C. Bernard, C. Bonneau, M. Kondratova, I. Kuperstein, A. Zinovyev, A.-M. Givel, M.-C. Parrini, V. Soumelis, A. Vincent-Salomon, and F. Mechta-Grigoriou, "Fibroblast heterogeneity and immunosuppressive environment in human breast cancer," Cancer Cell **33**(3), 463–479 (2018).

[32]S. Affo, A. Nair, F. Brundu, A. Ravichandra, S. Bhattacharjee, M. Matsuda, L. Chin, A. Filliol, W. Wen, X. Song, A. Decker, J. Worley, J. M. Caviglia, L. Yu, D. Yin, Y. Saito, T. Savage, R. G. Wells, M. Mack, L. Zender, N. Arpaia, H. E. Remotti, R. Rabadan, P. Sims, A.-L. Leblond, A. Weber, M.-O. Riener, B. R. Stockwell, J. Gablomme, J. M. Llovet, R. Kalluri, G. K. Michalopoulos, E. Seki, D. Sia, X. Chen, A. Califano, and R. F. Schwabe, "Promotion of cholangiocarcinoma growth by diverse cancer-associated fibroblast subpopulations," Cancer Cell **39**(6), 866–882.e11 (2021).

[33]I. Elia, J. H. Rowe, S. Johnson, S. Joshi, G. Notarangelo, K. Kurmi, S. Weiss, G. J. Freeman, A. H. Sharpe, and M. C. Haigis, "Tumor cells dictate anti-tumor immune responses by altering pyruvate utilization and succinate signaling in CD8+ T cells," Cell Metab. **34**(8), 1137–1150 (2022).

[34]L. Pan, J. J. Chou, and T. Fu, "Editorial: Targeting TNF/TNFR signaling pathways," Front. Pharmacol. **13**, 1120954 (2023).

[35]S. Hayward, M. Gachehiladze, N. Badr, R. Andrijes, G. Molostvov, L. Paniushkina, B. Sopikova, Z. Slobodová, G. Mgebrishvili, N. Sharma, Y. Horimoto, D. Burg, G. Robertson, A. Hanby, F. Hoar, D. Rea, B. L. Eckhardt, N. T. Ueno, I. Nazarenko, H. M. Long, S. van Laere, A. M. Shaaban, and F. Berditchevski, "The CD151-midkine pathway regulates the immune microenvironment in inflammatory breast cancer," J. Pathol. **251**(1), 63–73 (2020).

[36]R. Yang, Y. Zhan, Y. Li, S.-Y. Dai, S.-W. He, C.-J. Ye, L.-D. Meng, D.-Q. Chen, C.-B. Dong, L. Chen, G. Chen, K.-R. Dong, K. Li, S. Zheng, J. Li, W. Yao, and R. Dong, "The cellular and molecular landscape of synchronous pediatric sialoblastoma and hepatoblastoma," Front. Oncol. **12**, 893206 (2022).

[37]J. Moslehi, A. H. Lichtman, A. H. Sharpe, L. Galluzzi, and R. N. Kitsis, "Immune checkpoint inhibitor-associated myocarditis: Manifestations and mechanisms," J. Clin. Invest. **131**(5), e145186 (2021).

[38]X. Ma, Y. Zhang, S. Wang, H. Wei, and J. Yu, "Immune checkpoint inhibitor (ICI) combination therapy compared to monotherapy in advanced solid cancer: A systematic review," J. Cancer **12**(5), 1318–1333 (2021).

[39]C. Li and K. Hua, "Dissecting the single-cell transcriptome network of immune environment underlying cervical premalignant lesion, cervical cancer and metastatic lymph nodes," Front. Immunol. **13**, 897366 (2022).

[40]H. Cai, L. Yan, N. Liu, M. Xu, and H. Cai, "IFI16 promotes cervical cancer progression by upregulating PD-L1 in immunomicroenvironment through STING-TBK1-NF-kB pathway," Biomed. Pharmacother. **123**, 109790 (2020).

[41]S. Tilborghs, J. Corthouts, Y. Verhoeven, D. Arias, C. Rolfo, X. B. Trinh, and P. A. van Dam, "The role of nuclear factor-kappa B signaling in human cervical cancer," Crit. Rev. Oncol. Hematol. **120**, 141–150 (2017).

[42]L. Yu, Y. Sun, J. Su, and X. Li, "Bismahanine exerts anticancer effects on human cervical cancer cells by inhibition of growth, migration and invasion via suppression of NF-kB signalling pathway," J. BUON. **26**(1), 644–698 (2021).

[43]Y. Zhang, Y. Zhao, Y. Ran, J. Guo, H. Cui, and S. Liu, "Alantolactone exhibits selective antitumor effects in HELA human cervical cancer cells by inhibiting cell migration and invasion, G2/M cell cycle arrest, mitochondrial mediated apoptosis and targeting Nf-kB signalling pathway," J. BUON. **24**(6), 2310–2315 (2019).

[44]Y. Lin, M. J. Smit, R. Havinga, H. J. Verkade, R. J. Vonk, and F. Kuipers, "Differential effects of eicosapentaenoic acid on glycerolipid and apolipoprotein B metabolism in primary human hepatocytes compared to HepG2 cells and primary rat hepatocytes," Biochim. Biophys. Acta **1256**(1), 88–96 (1995).

[45]Z. Wang, Z. Zhang, K. Zhang, Q. Zhou, S. Chen, H. Zheng, G. Wang, S. Cai, F. Wang, and S. Li, "Multi-omics characterization of a glycerolipid metabolism-related gene enrichment score in colon cancer," Front. Oncol. **12**, 881953 (2022).

[46]X. Yang, X. Duan, Z. Xia, R. Huang, K. He, and G. Xiang, "The regulation network of glycerolipid metabolism as coregulators of immunotherapy-related myocarditis," Cardiovasc. Ther. **2023**, 8774971.

[47]Y. Naito, Y. Yoshioka, and T. Ochiya, "Intercellular crosstalk between cancer cells and cancer-associated fibroblasts via extracellular vesicles," Cancer Cell Int. **22**(1), 367 (2022).

[48]L. Zheng, Q. Liu, R. Li, S. Chen, J. Tan, L. Li, X. Dong, C. Huang, T. Wen, and J. Liu, "Targeting MDK abrogates IFN-γ-elicited metastasis incancers of various origins," Front. Oncol. **12**, 885656 (2022).

[49]H.-S. Moon, W. I. Park, S. H. Sung, E.-A. Choi, H.-W. Chung, and B. H. Woo, "Immunohistochemical and quantitative competitive PCR analyses of midkine and pleiotrophin expression in cervical cancer," Gynecol. Oncol. **88**(3), 289–297 (2003).

[50]R. Qureshi, H. Arora, and M. A. Rizvi, "EMT in cervical cancer: Its role in tumour progression and response to therapy," Cancer Lett. **356**(2), 321–331 (2015).

[51]X.-F. Hu, J. Yao, S.-G. Gao, Y.-T. Yang, X.-Q. Peng, and X.-S. Feng, "Midkine and syndecan-1 levels correlate with the progression of malignant gastric cardiac adenocarcinoma," Mol. Med. Rep. **10**(3), 1409–1415 (2014).

[52]A. Datta, C. West, J. P. B. O'Connor, A. Choudhury, and P. Hoskin, "Impact of hypoxia on cervical cancer outcomes," Int. J. Gynecol. Cancer **31**(11), 1459–1470 (2021).

[53]X. Zuo, L. Li, and L. Sun, "Plantamajoside inhibits hypoxia-induced migration and invasion of human cervical cancer cells through the NF-κB and PI3K/akt pathways," J. Recept. Signal Transduction Res. **41**(4), 339–348 (2021).

[54]L. Qiang, M. T. Hoffman, L. R. Ali, J. I. Castillo, L. Kageler, A. Temesgen, P. Lenehan, S. J. Wang, E. Bello, V. Cardot-Ruffino, G. A. Uribe, A. Yang, M. Dougan, A. J. Aguirre, S. Raghavan, M. Pelletier, V. Cremasco, and S. K. Dougan, "Transforming growth factor-β blockade in pancreatic cancer enhances sensitivity to combination chemotherapy," Gastroenterology **165**(4), 874–890.e10 (2023).

[55]D. Huang and C. Li, "circ-ACACA promotes proliferation, invasion, migration and glycolysis of cervical cancer cells by targeting the miR-582-5p/ERO1A signaling axis," Oncol. Lett. **22**(5), 795 (2021).

[56]C. S. Fjeldbo, E.-K. Aarnes, E. Malinen, G. B. Kristensen, and H. Lyng, "Identification and validation of reference genes for RT-qPCR studies of hypoxia in squamous cervical cancer patients," PLoS One **11**(5), e0156259 (2016).

[57]L. Liu, S. Li, Y. Qu, H. Bai, X. Pan, J. Wang, Z. Wang, J. Duan, J. Zhong, R. Wan, K. Fei, J. Xu, L. Yuan, C. Wang, P. Xue, X. Zhang, Z. Ma, and J. Wang, "Ablation of ERO1A induces lethal endoplasmic reticulum stress responses and immunogenic cell death to activate anti-tumor immunity," Cell Rep. Med. **4**, 101206 (2023).

[58]L. Liu, C. Wang, S. Li, Y. Qu, P. Xue, Z. Ma, X. Zhang, H. Bai, and J. Wang, "ERO1L is a novel and potential biomarker in lung adenocarcinoma and shapes the immune-suppressive tumor microenvironment," Front. Immunol. **12**, 677169 (2021).

[59]S. Mariathasan, S. J. Turley, D. Nickles, A. Castiglioni, K. Yuen, Y. Wang, E. E. Kadel, H. Koeppen, J. L. Astarita, R. Cubas, S. Jhunjhunwala, R. Banchereau, Y. Yang, Y. Guan, C. Chalouni, J. Ziai, Y. Şenbabaoğlu, S. Santoro, D. Sheinson, J. Hung, J. M. Giltnane, A. A. Pierce, K. Mesh, S. Lianoglou, J. Riegler, R. A. D. Carano, P. Eriksson, M. Höglund, L. Somarriba, D. L. Halligan, M. S. van der Heijden, Y. Loriot, J. E. Rosenberg, L. Fong, I. Mellman, D. S. Chen, M. Green, C. Derleth, G. D. Fine, P. S. Hegde, R. Bourgon, and T. Powles, "TGFβ attenuates tumour response to PD-L1 blockade by contributing to exclusion of T cells," Nature **554**(7693), 544–548 (2018).

[60]J. Yang, J. Zhang, S. Na, Z. Wang, H. Li, Y. Su, L. Ji, X. Tang, J. Yang, and L. Xu, "Integration of single-cell RNA sequencing and bulk RNA sequencing to reveal an immunogenic cell death-related 5-gene panel as a prognostic model for osteosarcoma," Front. Immunol. **13**, 994034 (2022).

[61]J. Cai, J. Hu, Z. Ye, L. Ye, L. Gao, Y. Wang, Q. Sun, S. Tong, J. Yang, and Q. Chen, "Immunogenic cell death-related risk signature predicts prognosis and characterizes the tumour microenvironment in lower-grade glioma," Front. Immunol. **13**, 1011757 (2022).

[62]Y. Hao, T. Stuart, M. H. Kowalski, S. Choudhary, P. Hoffman, A. Hartman, A. Srivastava, G. Molla, S. Madad, C. Fernandez-Granda, and R. Satija, "Dictionary learning for integrative, multimodal and scalable single-cell analysis," Nat. Biotechnol. **42**, 293 (2024).

[63]I. Korsunsky, N. Millard, J. Fan, K. Slowikowski, F. Zhang, K. Wei, Y. Baglaenko, M. Brenner, P.-R. Loh, and S. Raychaudhuri, "Fast, sensitive and accurate integration of single-cell data with harmony," Nat. Methods **16**(12), 1289–1296 (2019).

[64]D. Aran, A. P. Looney, L. Liu, E. Wu, V. Fong, A. Hsu, S. Chak, R. P. Naikawadi, P. J. Wolters, A. R. Abate, A. J. Butte, and M. Bhattacharya, "Reference-based analysis of lung single-cell sequencing reveals a transitional profibrotic macrophage," Nat. Immunol. **20**(2), 163–172 (2019).

[65]X. Zhang, Y. Lan, J. Xu, F. Quan, E. Zhao, C. Deng, T. Luo, L. Xu, G. Liao, M. Yan, Y. Ping, F. Li, A. Shi, J. Bai, T. Zhao, X. Li, and Y. Xiao, "CellMarker: A manually curated resource of cell markers in human and mouse," Nucl. Acids Res. **47**(D1), D721–D728 (2019).

[66]C. Trapnell, D. Cacchiarelli, J. Grimsby, P. Pokharel, S. Li, M. Morse, N. J. Lennon, K. J. Livak, T. S. Mikkelsen, and J. L. Rinn, "The dynamics and regulators of cell fate decisions are revealed by pseudotemporal ordering of single cells," Nat. Biotechnol. **32**(4), 381–386 (2014).

[67]S. Jin, C. F. Guerrero-Juarez, L. Zhang, I. Chang, R. Ramos, C.-H. Kuan, P. Myung, M. V. Plikus, and Q. Nie, "Inference and analysis of cell-cell communication using CellChat," Nat. Commun. **12**(1), 1088 (2021).

[68]S. Aibar, C. B. González-Blas, T. Moerman, V. A. Huynh-Thu, H. Imrichova, G. Hulselmans, F. Rambow, J.-C. Marine, P. Geurts, J. Aerts, J. van den Oord, Z. K. Atak, J. Wouters, and S. Aerts, "SCENIC: Single-cell regulatory network inference and clustering," Nat. Methods **14**(11), 1083–1086 (2017).